ACS OMEGA

http://pubs.acs.org/journal/acsodf

Article

Injectable Hydrogel Based on Gellan Gum/Silk Sericin for Application as a Retinal Pigment Epithelium Cell Carrier

Soo in Kim, Ga Yeong Jeon, Se Eun Kim, Seung Ho Choe, Seung Jae Kim, Jin Sol Seo, Tae Woong Kang, Jeong Eun Song, and Gilson Khang*

Cite This: *ACS Omega* 2022, 7, 41331−41340

Read Online

ACCESS | Metrics & More | Article Recommendations

ABSTRACT: The damage to retinal pigment epithelium (RPE) cells can lead to vision loss and permanent blindness. Therefore, an effective therapeutic strategy has emerged to replace damaged cells through RPE cell delivery. In this study, we fabricated injectable gellan gum (GG)/silk sericin (SS) hydrogels as a cell carrier by blending GG and SS. To determine the appropriate concentration of SS for human RPE ARPE-19, 0, 0.05, 0.1, and 0.5% (w/v) of SS solution were blended in 1% (w/v) GG solution (GG/SS 0%, GG/SS 0.05%, GG/SS 0.1%, and GG/SS 0.5%, respectively). The physical and chemical properties were measured through Fourier-transform infrared spectroscopy, scanning electron microscopy, mass swelling, and weight loss. Also, viscosity, injection force, and compressive tests were used to evaluate mechanical characteristics. Cell proliferation and differentiation of ARPE-19 were evaluated using quantitative dsDNA analysis and real-time polymerase chain reaction, respectively. The addition of SS gave GG/SS hydrogels a compressive strength similar to that of natural RPE tissue, which may well support the growth of RPE and enhance cell proliferation and differentiation. In particular, the GG/SS 0.5% hydrogel showed the most similar compressive strength (about 10 kPa) and exhibited the highest gene expression related to ARPE-19 cell proliferation. These results indicate that GG/SS 0.5% hydrogels can be a promising biomaterial for cell delivery in retina tissue engineering.

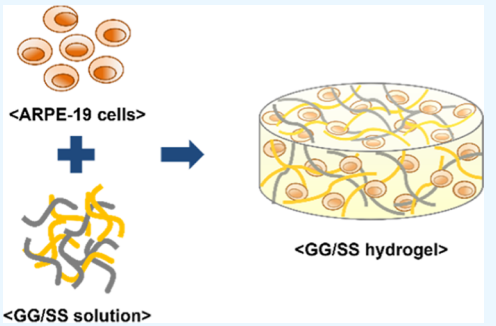

1. INTRODUCTION

Retinal pigment epithelial (RPE) cells, the outermost layer of the retina, play a major role in the maintenance of retinal homeostasis and visual function.[1] Because RPE cells are unable to regenerate damaged cells, dysfunction or degeneration of RPE cells can cause various retinal diseases related to vision impairment and lead to permanent loss of visual function. Particularly, age-related macular degeneration is currently the leading cause of blindness in developed countries.[2,3] As a treatment for these diseases, transplantation of RPE cells into the subretinal space emerged as a potential alternative to replace damaged RPE cells.[4,5] However, direct injection of the RPE cell suspension is accompanied by a low percentage of cell attachment and survival and fibrosis leading to significant cell death.[6] Also, the considerable therapeutic effect of cell transplantation has not yet been confirmed.[4,7]

To overcome these limitations, different biomaterials such as decellularized tissue, hyaluronic acid, alginate, polyethylene glycol, and so on and various types of scaffolds have been studied to promote retinal tissue formation in addition to integration into host tissues.[8,9] Among various scaffolds, injectable hydrogels composed of natural polymers have attracted much attention as a promising cell delivery system because of their unique characteristics such as excellent biocompatibility and a three-dimensional (3D) network similar to that of natural soft tissue.[10−12] In addition, injectability can fill irregular tissue defects and uniformly distribute encapsulated cells with a minimally invasive procedure.[13,14]

Gellan gum (GG) is a nature-derived anionic polysaccharide with repeating units consisting of 1,3-β-D-glucose, 1,4-β-D-glucuronic acid, 1,4-β-D-glucose, and 1,4-α-L-rhamnose. GG has been widely used for tissue engineering due to heat and acid stability, excellent biocompatibility, biodegradability, nontoxicity, tunable mechanical properties, and thermosensitive gelling characteristics.[15,16] Because of these properties, it has also been extensively utilized for the development of ocular drug delivery systems.[17−19] GG can physically be cross-linked by cations. Specifically, divalent cations (Mg^{2+} and Ca^{2+}) provide direct bridges between pairs of double helices, and monovalent cations (Na^{+} and K^{+}) induce aggregation by reducing electrostatic repulsions between carboxyl groups.[20]

Received: August 9, 2022
Accepted: October 21, 2022
Published: November 2, 2022

https://doi.org/10.1021/acsomega.2c05113
ACS Omega 2022, 7, 41331−41340

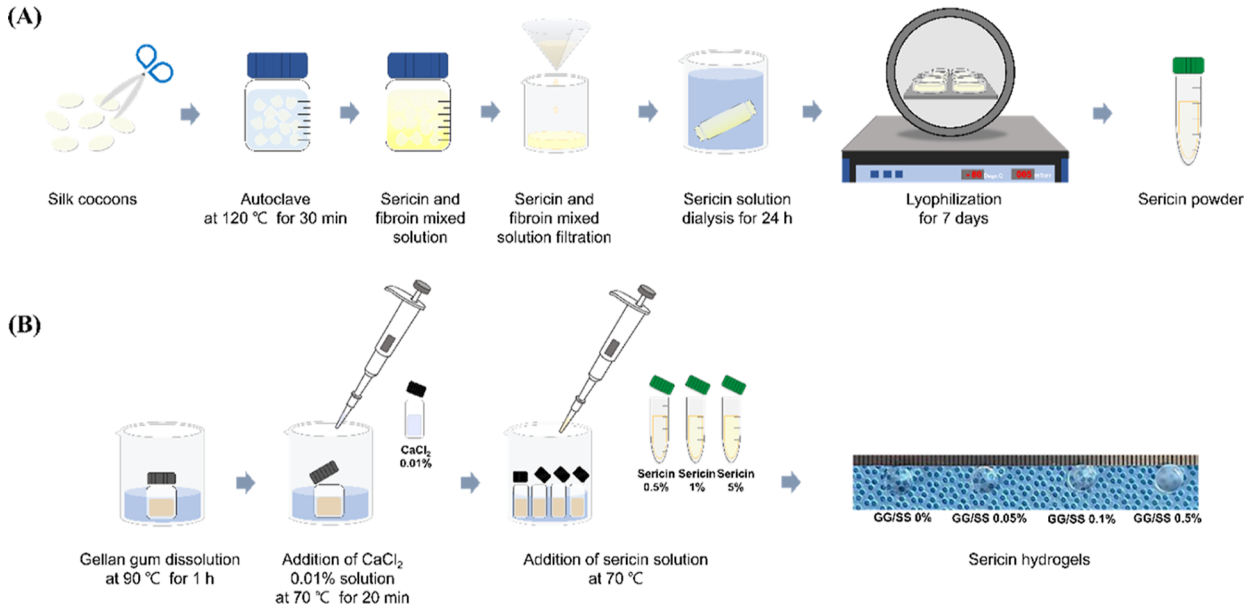

Figure 1. Schematic of the GG/SS hydrogel fabrication procedure: (A) SS powder preparation and (B) GG/SS scaffold formation.

GG's high gelation temperature, however, makes it difficult to homogeneously disperse GG at the target site during injection, and it is difficult to encapsulate cells at physiological temperature (~37.5 °C). In addition, the low cell affinity of GG inhibits cell survival and growth.[21−23]

Silk sericin (SS) is a glue-like glycoprotein that envelops fibroin fibers together to form silk cocoons.[24] SS mainly consists of hydrophilic amino acids with polar side chains, especially serine and aspartic acid, thus enabling easy cross-linking and blending with other polymers and promoting cell attachment.[25] SS is also known to have diverse bioactivities, such as antioxidant, antibacterial, and anticoagulating activity, moisturizing activity, promotion of cell growth, and differentiation of mammalian cells.[26,27] Thus, SS has been widely used in soft tissue engineering such as in cornea and skin owing to these outstanding characteristics in biomedical applications.[28−31] It has also been reported that sericin enhanced the proliferation of RPE cells and had a significant effect on the maturation of RPE cells by activating the NF-κB pathway.[32] Earlier reports claimed that SS was responsible for an immune response. In recent studies, the immune response of SS proved to be dependent on physical association with fibroin−silk fibers. Therefore, SS itself has no immunogenicity.[25,33] However, SS forms fragile scaffolds that are not suitable for biomedical applications,[34,35] and the use of a cross-linking agent such as glutaraldehyde and genipin, the main fabricating method of SS hydrogels, can cause toxicity.[36] To fabricate the stable SS hydrogels, cross-linking and blending with other substances such as poly(vinyl alcohol),[37] chitosan,[38] and gelatin[26] are often investigated.

Therefore, we prepared GG/SS hydrogels that can complement the insufficient cell affinity of GG and the poor mechanical properties of SS. The purpose of this work was to fabricate GG/SS scaffolds with appropriate mechanical strength and bioactivity for retinal tissue engineering. To evaluate the optimized content of SS for retinal regeneration, the 3D GG/SS scaffolds were prepared by adding SS solution into a fixed concentration of GG solution. Subsequently, they have investigated both characterization and in vitro for their potential in tissue engineering applications.

2. MATERIALS AND METHODS

2.1. Silk Sericin Extraction. SS was extracted from *Bombyx mori* cocoons according to a previously described method (Figure 1).[39,40] Briefly, 20 g of silk cocoons was cut into small pieces and autoclaved in deionized water (1 g of cocoons/50 mL of water) at 120 °C for 30 min. After autoclaving, the SS and fibroin mixed solution was filtrated through a Whatman filter (Advantec, Japan) to remove fibroin. Then, the SS solution was dialyzed using a dialysis bag (14,000 MWCO, Sigma-Aldrich, USA) against deionized water at room temperature for 24 h. Finally, the dialysate was lyophilized (−80 °C, 005 mTorr) for 7 days, and SS powder was stored at −4 °C until use.

2.2. Preparation of GG/SS Hydrogels. Four hydrogel solutions of different GG/SS weight ratios were prepared. Briefly, 100 mg of low-acyl GG (GG; Gelzan CM, Sigma-Aldrich, USA) was dissolved in 9 mL of distilled water under constant stirring for 1 h at 90 °C. The temperature was then lowered to 70 °C, and 0.01% (w/v) of calcium chloride ($CaCl_2$, Sigma-Aldrich, USA) as a cross-linking agent was homogeneously mixed in the GG solution for 20 min. The different amounts of SS powder (0.5, 1, and 5%) were completely dissolved in 1 mL of distilled water at 70 °C. The prepared SS solution was added in the GG solution to fabricate total 1% (w/v) GG with 0, 0.05, 0.1, and 0.5% (w/v) SS, and the blended solution was stirred for 20 min. The samples were specified as GG/SS 0%, GG/SS 0.05%, GG/SS 0.1%, and GG/SS 0.5%, respectively. The sample named GG/SS 0% was added with distilled water instead of the SS solution. 7 mL of the prepared hydrogel solutions was poured into Petri dishes (50 mm × 10 mm, SPL Life Sciences Co., Ltd., South Korea) and solidified at room temperature for 10 min. After gelation was completed, cylindrical-shaped hydrogels with a diameter of 6 mm and a height of approximately 3 mm were prepared using a biopsy punch (Kai Medical Biopsy Punch, Japan).

2.3. Fourier-Transform Infrared Spectroscopy. The composition variation of the fabricated hydrogels was analyzed using an attenuated total reflectance-Fourier-transform infrared spectrometer (PerkinElmer, Boston, MA, USA) in the range of

https://doi.org/10.1021/acsomega.2c05113
ACS Omega 2022, 7, 41331−41340

400−4000 cm^{-1}. All hydrogels were frozen at −80 °C overnight and further lyophilized for the measurement.

2.4. Scanning Electron Microscopy. The morphological evaluation of the hydrogels was performed by scanning electron microscopy (SEM) (Bio-LV SEM, Japan, HITACHI). Before SEM imaging, the hydrogels were sequentially stored at 4, − 20, and −80 °C overnight and lyophilized (−80 °C, 005 mTorr) for 48 h. The dried samples were cut with single-edge blades (Dorco Living Vina Co Ltd., South Korea) and coated using a plasma sputter (Model SC500k, Emscope, UK). The pore diameters were measured using ImageJ software (Java-based image software, LOCI, University of Wisconsin).

2.5. Physicochemical Studies. *2.5.1. Mass Swelling Ratio.* The prepared scaffolds were immersed in phosphate buffered saline (PBS, pH 7, Gibco) at 37 °C for 24 h. The wet weight of the samples was measured (W_w) after the initial removal of the redundant PBS and lyophilized (−80 °C, 005 mTorr) for 48 h. The mass of the dried samples was recorded (W_f), and the mass swelling ratio was determined using the following equation.

$$\text{mass swelling ratio} = \frac{W_w}{W_f}$$

2.5.2. Weight Loss (%). The weight loss (%) of the hydrogels was measured on days 7, 14, 21, and 28. The prepared scaffolds were immersed in PBS at 37 °C for 24 h. The initial weights of the samples (W_i) were recorded. Then, the hydrogels were immersed in 1 mL of PBS at 37 °C. At the specific time points, the weight of the hydrogels (W_s) was recorded. PBS was exchanged every 3 days. The weight loss (%) was calculated using the following equation

$$\text{weight loss (\%)} = \frac{W_i - W_s}{W_i} \times 100(\%)$$

2.6. Mechanical Characterization. *2.6.1. Rheological Measurements.* The viscosity and gelation temperature of prepared hydrogel solutions were measured using a viscometer (AMETEK Brookfield, USA). A water circulation bath (VCB 07, JONGRO Industrial Co., Ltd, South Korea) was set at 40 °C, and 8 mL of GG/SS solutions was added to the viscometer. The temperature was gradually lowered until the water bath temperature reached 20 °C. The router speed was set at 1 rpm, and cone and plate spindles (LV-04 spindle, AMETEK Brookfield, USA) were used for this study.

2.6.2. Injectability Test. The injectability of the hydrogel was investigated by slightly modifying the method reported in the previous study.[41] 500 μL of the prepared hydrogel solutions was loaded into a syringe (26G1/2 needle, Korea Vaccine Co., Ltd, South Korea), and the samples were stored at room temperature for 5 min. Then, the syringe was loaded onto a custom-made bracket. The injectability test was performed using a texture analyzer (FTC, Sterling, Virginia, USA) at a rate of 20 mm/min^{-1} with the needle's tip immersed in the PBS to mimic the in vivo injection environment.

2.6.3. Compression Test. Mechanical characterization was studied using the texture analyzer (FTC, Sterling, Virginia, USA) with a 10 N load cell. Cylindrical samples with 8 mm diameter and 3 mm height were immersed in PBS at 37 °C for 24 h before the compression test. The stress−strain curve of the samples was drawn, and the initial elastic modulus was calculated at 5−10% strain.

2.7. In Vitro Study. *2.7.1. Hydrogel 3D Cell Culture.* Human RPE ARPE-19 (ATCC CRL-2302, ATCC) was cultured in Dulbecco's modified Eagle's medium/nutrient mixture F-12 (DMEM F-12, Gibco) supplemented with 10% fetal bovine serum (FBS, Gibco) and 1% antibiotic−antimycotic (100×) (Anti-Anti, Gibco) at 37 °C under a humidified atmosphere of 95% air and 5% CO_2. The cell culture medium was changed every 3 days, and the cells were subcultured until they reached a sufficient level for seeding in the hydrogels. The hydrogel solutions were prepared as described in Section 2.2 and were filtered through a 0.45 μm pore size filter (Millex Syringe Filters, Merck Millipore, Darmstadt, Germany) to remove impurities. Before the experiments, all of the materials were autoclaved for use. Cultured ARPE-19 cells were trypsinized using a 0.5% trypsin solution (Gibco, USA). The cell pellet with a density of 1×10^5 cells/mL was mixed with the hydrogel solution at 37 °C, and the mixture was poured into Petri dishes. The cell-laden hydrogel solutions were solidified for 10 min at room temperature. The fabricated cell-laden hydrogels were punched with a 6 mm biopsy punch (Kai Medical, HI, USA) to obtain 6 mm-diameter discs with 4 mm height and transferred to a 24-well plate. The cell culture medium was added, and the hydrogels were incubated at 37 °C in a 5% CO_2 incubator. The medium was changed every 3 days.

2.7.2. Cytotoxicity Assay. The cytotoxicity of the GG/SS hydrogels was evaluated by the extraction test reported in the previous study with a slight modification.[42] First, 2.6 mL of the fabricated hydrogel solutions was molded into a silicone mold of 100 μL and solidified at room temperature for 10 min. The prepared hydrogels were immersed in 10 mL of Roswell Park Memorial Institute (RPMI) medium (Gibco, USA) supplemented with 10% FBS (Gibco, USA) and 1% penicillin/streptomycin (PS, Gibco, USA) at 37 °C in a water bath for 24 h. Autoclaved latex was chopped into pieces for the positive control (2.5 cm^2/mL) and incubated at 37 °C in a water bath for 24 h. After the incubation period, the extracted supernatant was filtered through a 0.45 μm pore size filter. A NIH/3T3 mouse embryo fibroblast (National Institute of Health, KCLB21658) obtained from the Korean Cell Line Bank (KCLB, Seoul, Korea) was used for this study. The cells were cultured in RPMI medium (Gibco, USA) supplemented with 10% FBS (Gibco, USA) and 1% penicillin/streptomycin (PS, Gibco, USA) at 37 °C with 5% CO_2. The cells were seeded ($n = 8$, 2×10^3 cells/well) on 96-well plates and were cultured for 48 h at 37 °C with 5% CO_2. The culture medium was removed after 48 h and replaced with the extraction fluid and stored under standard culture conditions (5% CO_2 and 37 °C) for 1, 2, and 3 days. At the specific times, the supernatant was removed, and 90 μL of cell culture medium and 10 μL of 3-(4,-dimethylthiazol-2-yl)-2,5-diphenyltetrazolium bromide (MTT; thiazolyl blue, 5 mg/mL in PBS, Amresco, TX, USA) solution were added to each well for 2 h at 37 °C in a 5% CO_2 incubator. Treatments were removed, and 100 μL of dimethyl sulfoxide (DMSO, Samchun Chemical, South Korea) was added to dissolve the formazan crystal. The absorbance was measured at 570 nm with a microplate reader (Synergy MX, Biotek, Vernusky, VT, USA). All the groups were normalized with the negative control (RPMI medium) to calculate cell viability (%).

2.7.3. dsDNA Content Analysis. The dsDNA content of the hydrogels was measured using the Quant-iT PicoGreen reagent (Life Technologies, USA) according to the manu-

https://doi.org/10.1021/acsomega.2c05113
ACS Omega 2022, 7, 41331−41340

facturer's instruction. Scaffolds were cultured for 3 and 28 days. At specific time points, the samples were washed with PBS and stored in a deep freezer. To induce cell lysis, the hydrogels were thawed at room temperature, and 1× TE buffer (10 mM Tris−HCl, 1 mM EDTA, pH 7.5) was added using a glass tissue grinder (Wheaton, USA) for homogenization. The solutions were transferred into a 96-well black plate (Cell Culture Plate, SPL Life Sciences Co., Ltd., South Korea), and the Quant-iT PicoGreen reagent was added to the samples in a 1:1 ratio. The samples were stored at room temperature for 5 min, and the dsDNA content quantification was measured with a microplate reader (BioTek Instruments, Inc., USA) at an excitation wavelength of 485/20 nm and an emission wavelength of 528/20 nm. The concentration of the solutions in the range of 0−2 μg/mL was used for the standard curve.

2.7.4. Live/Dead Assay. The cell viability and proliferation on different GG/SS scaffolds were assessed by live/dead staining. The cell-laden scaffolds were stained using the live/dead cell imaging kit (Invitrogen, USA) according to the kit protocol. After 3 and 14 days of culture, the hydrogels were transferred to a confocal dish (SPL Life Sciences, Co., Ltd., South Korea) and stained with calcein AM and ethidium homodimer for 30 min at 37 °C in a 5% CO_2 incubator. The fluorescence was visualized using a super-resolution confocal laser scanning microscope (SR CLSM < LSM 880 with Airyscan, Carl Zeiss, Germany) with a Z-stack mode. All measured thicknesses were unified to 200 μm, and the fluorescence intensity of live/dead staining was characterized using ImageJ software.

2.7.5. Real-Time Polymerase Chain Reaction. The samples were washed with PBS three times and treated with Trizol (Takara Bio, Inc., Japan) using a glass tissue grinder (Wheaton, USA) for cell lysis. The homogenized solution was transferred to a 1.5 mL Eppendorf tube (EP tube), and chloroform (SAMCHUN Chemicals, South Korea) was mixed. The samples were centrifuged at 12,000 rpm at 4 °C for 15 min, and the supernatant was transferred into a new EP tube. 2-Propanol (Sigma-Aldrich, USA) was added to the solution and stored at −20 °C overnight. The samples were centrifuged at 12,000 rpm at 4 °C for 15 min, and the supernatant was discarded. Then, obtained RNA was washed by adding 75% ethanol, and the samples were centrifuged at 7500 rpm at 4 °C for 5 min. The supernatant was discarded, and RNase−DNase-free water (Gibco, USA) was used to dilute the obtained mRNA. The concentration was measured using a biospectrophotometer (Eppendorf, USA), and cDNA was synthesized with a TOPscript RT DryMIX (dT18 plus) (Enzynomics, South Korea) and PCR thermocycler (Takara Bio, Inc., Japan). Real-time polymerase chain reaction (RT-PCR) was performed with an SYBR Green PCR Master Mix (Applied Biosystems) and StepOnePlus Real-Time PCR system (Applied Biosystems). RPE-specific primers such as cellular retinaldehyde-binding protein (CRALBP), RPE-specific 65 kDa (RPE65), rhodopsin (RHODO), microphthalmia-associated transcription factor (MITF), atrial natriuretic peptide receptor (NPR-A), and collagen type I (COL I) were used for this study.[43] The gene expression was normalized by the housekeeping gene, glyceraldehyde 3-phosphate dehydrogenase (GAPDH), and calculated with the $2^{-\triangle\triangle CT}$ method.[44] The primer sequences are shown in Table 1.

2.8. Statistical Analysis. All data were expressed as the mean ± standard deviation (SD). Results were statistically analyzed by one-way analysis of variance (one-way ANOVA test), using GraphPad Prism 5.0 (GraphPad Software, La Jolla, CA, USA) to identify the level of significance among different samples. The differences were considered significant at $p < 0.05(*)$, $p < 0.01(**)$, and $p < 0.001(***)$.

Table 1. Primer Sequences Used in RT-PCR

primer	primer sequence
GAPDH	F: 5′-GGC ACA GTC AAG GCT GAG AAT G-3′
	R: 5′-ATG GTG GTG AAG ACG CCA GTA-3′
CRALBP	F: 5′-CGT GGC GGA GAG GGT GCA AG-3′
	R: 5′-GGT GCA GCG GAC AGC CTC TG-3′
RPE65	F: 5′-CGT ATG GAC TTG GCT TGA ATC-3′
	R: 5′-CTG GGT GAG AAA CAA AGA TGG-3′
RHODO	F: 5′-TCA TCA TGG TCA TCG CTT TC-3′
	R: 5′-CAT GAA GAT GGG ACC GAA GT-3′
MITF	F: 5′-AGC TTG CCA TGT CCA AAC CAG-3′
	R: 5′-TTC ATA CTT GGG CAC TCG CTC T-3′
NPR-A	F: 5′-AGA GGG AGA ACC TGA CCG ACC G-3′
	R: 5′-ACG ATT CTG GAA TTC CTG ATA CTC-3′
COL I	F: 5′-CTG ACT GGA AGA GCG GAG AGT AC-3′
	R: 5′-CCA TGT CGC AGA AGA CCT TGA-3′

3. RESULTS AND DISCUSSION

3.1. FT-IR Analysis. Fourier-transform infrared (FT-IR) analysis was performed to confirm the chemical structures of GG, SS, and GG/SS matrices in the wavenumber range of 4000−400 cm^{-1} (Figure 2). The pure SS exhibited characteristic peaks at 3276 cm^{-1} which correspond to the overlapping of N−H and O−H stretching vibrations. Also, SS had specific peaks at 1619 and 1516 cm^{-1} representing amide I related to the β-sheet structure and amide II (C═O stretching, N−H bending) bands, along with an amide III (C−N stretching) peak at 1240 cm^{-1}.[45] In the GG's spectrum, the broadband at 3600−3000 cm^{-1} centered at 3296 cm^{-1} was associated with stretching vibration of O−H, and the characteristic peaks at 2920 cm^{-1} were attributed to the C−H_2 stretching. The peaks around 1606 and 1407 cm^{-1} were ascribed to the asymmetric and symmetric stretching of carboxyl groups, respectively, and 1015 cm^{-1} presented the stretching vibration of C−O.[46] As the SS content increases, the bands related to amide I shift from 1619 to 1605 cm^{-1}, suggesting a structure transition from the β-sheet to aggregated strands.[47] However, in the FT-IR spectra of the GG/SS 0.5% scaffold, the bands related to amide I shifted from 1619 to 1644 cm^{-1}, demonstrating a random coil conformation of SS formed.[48]

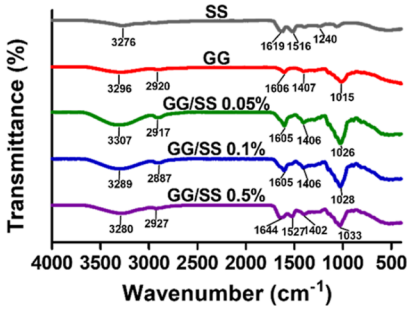

Figure 2. FT-IR spectra of SS, GG, and GG/SS hydrogel powder.

3.2. Morphology. The pore size is a crucial property for a scaffold because it affects cell adhesion and proliferation, supply of nutrients and oxygen, and removal of metabolic

https://doi.org/10.1021/acsomega.2c05113
ACS Omega 2022, 7, 41331−41340

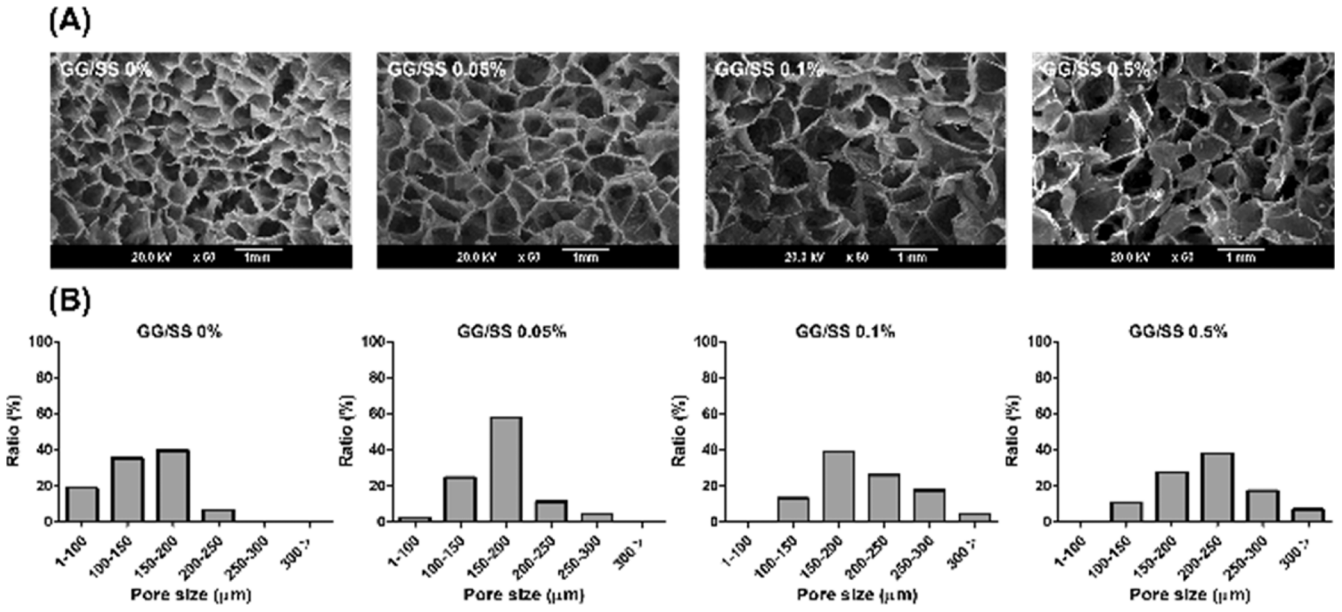

Figure 3. SEM images of scaffolds: (A) porous microstructure of GG/SS scaffolds and (B) pore size distribution for four samples.

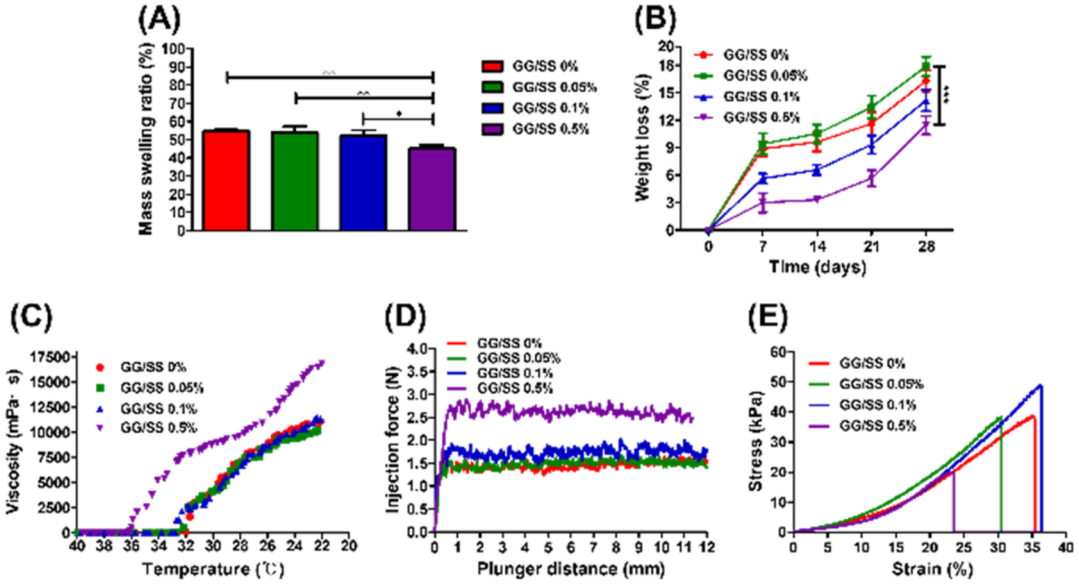

Figure 4. Physicochemical and mechanical characterization of the GG/SS scaffolds: (A) mass swelling ratio (%), (B) weight loss (%), (C) viscosity, (D) injection force, and (E) compressive stress−strain curve [the values are mean ± SD (n = 3), $p < 0.05$(*), $p < 0.01$(**), and $p < 0.001$(***)].

substances.[49] The porous microstructure of GG/SS scaffolds was measured by SEM images (Figure 3A). The pore diameters of the GG/SS scaffolds with 0, 0.05, and 0.1% SS were in the range of 150−200 μm with mean sizes 141.52 ± 37.38, 171.24 ± 40.87, and 205.70 ± 52.52 μm, respectively. Also, the pore sizes in GG/SS 0.5% were mainly in the range of 200−250 μm with a mean size of 223.21 ± 56.95 μm (Figure 3B). As a result, the higher SS content showed increased pore sizes. The pore size depends on the size of the ice crystals formed during freezing. Therefore, due to the hydrophilicity of SS, a high concentration of SS formed larger water droplets during the freezing process, and it seemed that large pores were introduced due to the slow temperature change.[50] In addition, it was reported that ARPE-19 enhanced cell attachment on larger-diameter fibers (approximately 1300 nm) in a previous study,[51] and macropores (>100 μm) play an important role in cell distribution, migration, and neovascularization.[52] Therefore, the GG/SS hydrogels can be suggested as a matrix for supporting the growth of RPE. However, the pore sizes of the freeze-dried hydrogels are slightly different from the pore sizes of the swollen hydrogels. In order to confirm the exact microstructure of the hydrogels, it is also recommended to observe the images of the swollen hydrogels.[53]

3.3. Physicochemical and Mechanical Analysis. The mass swelling ratio of hydrogels is an important characteristic that determines the degradation rate and mechanical and viscoelastic properties.[54] To investigate the swelling behavior according to SS contents, hydrogels with different GG/SS ratios were measured. The swelling behavior depends on their structural properties such as the interaction between solvents, cross-link density, and hydrophilicity.[55] Thus, due to the

https://doi.org/10.1021/acsomega.2c05113
ACS Omega 2022, 7, 41331−41340

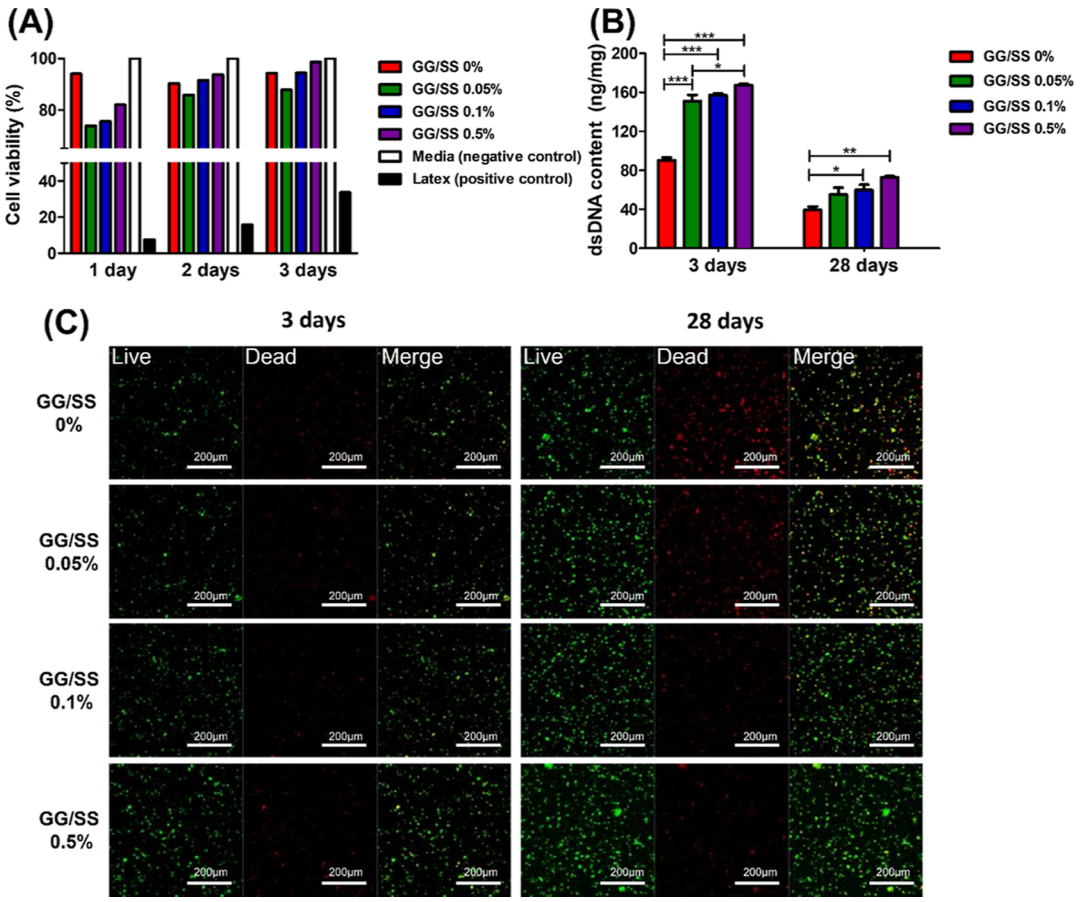

Figure 5. Cytocompatibility assessment: (A) cytotoxicity, (B) dsDNA quantification, and (C) live/dead staining. Live cells were stained in green, and dead cells were stained in red [the values are mean ± SD (n = 3), $p < 0.05$(*), $p < 0.01$(**), and $p < 0.001$(***)].

hydrophilicity of SS, it was expected that the mass swelling ratio would increase as the content of SS increased. However, the mass swelling ratio in scaffolds decreased from 54.53 to 45.02% with the increase in SS contents (Figure 4A). These results suggested that other structural characteristics of SS had a greater effect on the swelling behavior. The pure GG showed a high weight loss rate compared to the SS-content scaffolds for 28 days (Figure 4B). As the SS concentration of gel increased from 0.05 to 0.5%, the corresponding weight loss ratios decreased, and especially GG/SS 0.5% showed the lowest weight loss rate in all hydrogels. On day 28, the weight loss of 0.5% of GG/SS was 11%, which is 5% lower than that of pure GG ($p < 0.001$). Therefore, the low weight loss rate of the SS-containing scaffolds is believed to be related to the low mass swelling.

In biomaterial implantation, the mechanical properties of the implanted material should be similar to those of the target tissue to promote optimal cell activity and transplant integration.[56] Gelation temperature according to different SS concentrations was measured by a sharp increase in viscosity (Figure 4C).[57] The GG/SS hydrogels with the concentration of SS in a range of 0−0.1% showed no significant difference in the gelation temperature. However, when the content of SS was increased to 0.5%, the gelation temperature was changed from 32 to 37 °C. Although the GG/SS 0.5 scaffold had the gelation temperature which was higher than that of other scaffolds, it showed proper gelation temperature (<37 °C) for cell encapsulation.[58] Following previous studies, the SS gelation was due to the transformation of the random coil of SS molecules into the β-sheet structure.[59,60] In this study, however, the GG/SS hydrogel was formed without change of the SS secondary structure, indicating that gel network formation of GG using $CaCl_2$ contributed greatly to the gelation.[61] Injectability is a significant parameter that confirms the usability of the hydrogel.[62] Therefore, the injection force of four hydrogels was evaluated (Figure 4D). The injection force first increased to approximately 1 mm displacement, which was then kept constant. Plateau values were about 1.5, 1.5, 1.8, and 2.8 N for the scaffolds GG/SS 0%, GG/SS 0.05%, GG/SS 0.1%, and GG/SS 0.5%, respectively. As with the gelation temperature, there was a significant difference in the GG/SS 0.5% hydrogel. Compressive strength was evaluated to confirm the hydrogel's ability to withstand intraocular pressure under compression.[63] Previous studies have demonstrated that the compressive modulus of the native retina is about 10−20 kPa.[64] The compressive stress−strain curves of the fabricated hydrogels were presented (Figure 4E). There was no noticeable change until the content of SS was increased from 0 to 0.1%. However, the compressive stress of GG/SS 0.5% decreased from 38 to 20 kPa compared to that of GG/SS 0%, and it was broken at about 24% strain. SS has poor mechanical stability due to its high content of random coils. Therefore, in previous experiments, the strength of the gel was enhanced by increasing the proportions of the β-sheet via bending, synthesis, and cross-linking agents, such as ethanol, genipin, and glutaraldehyde.[27,65,66] These results suggest that the random coils of SS decrease the strength of the GG/SS hydrogel.

https://doi.org/10.1021/acsomega.2c05113
ACS Omega 2022, 7, 41331−41340

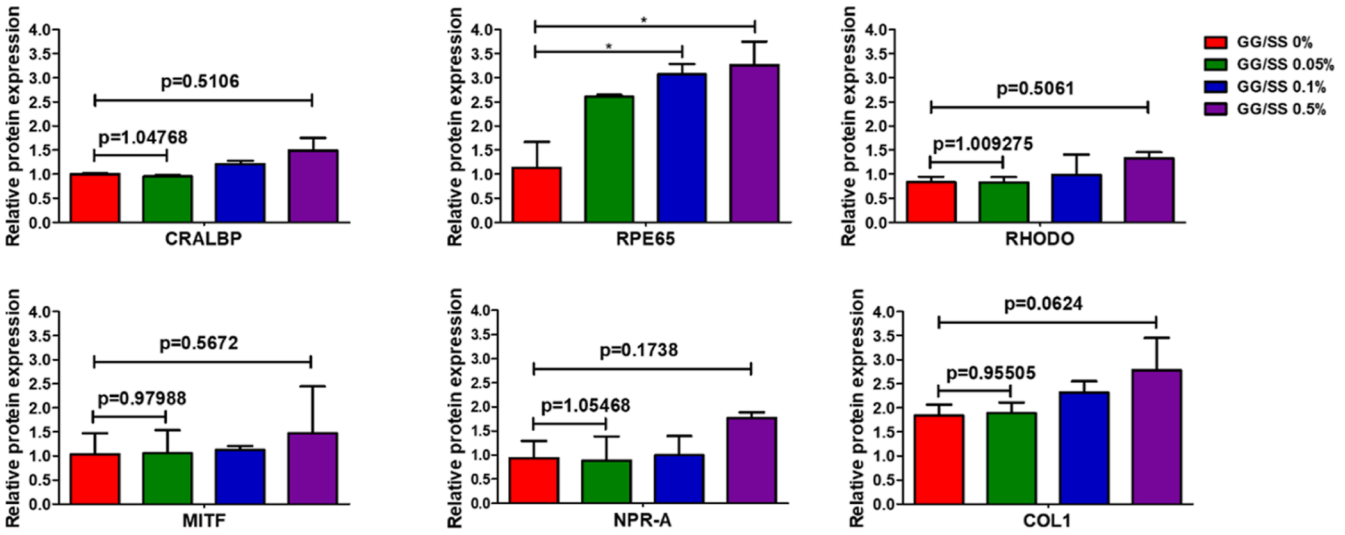

Figure 6. RT quantitative PCR analysis of RPE-related gene expression of ARPE-19 encapsulated in the hydrogels at 28 days [the values are mean ± SD (n = 3), $p < 0.05$(*), $p < 0.01$(**), and $p < 0.001$(***)].

3.4. In Vitro Study. *3.4.1. Cytocompatibility Test.* The cytotoxicity study for GG/SS hydrogels was performed on NIH/3T3 cells by MTT assay. The GG/SS hydrogels exhibited a higher cell proliferation rate compared to the pure GG hydrogel (Figure 5A). On day 1, the GG/SS 0% showed the highest cell viability at 93% in all hydrogels. In the following 2 days, however, the hydrogels containing SS showed a much higher proliferation rate of about 10% or more than that of the GG/SS 0% hydrogels. Finally, on day 3, the GG/SS 0.5% showed the highest cell viability among these hydrogels. In previous studies, non-cytotoxic effects of SS have been demonstrated using several types of cells.[67−69] Therefore, it is expected that GG/SS 0.5% supported longer-term cell proliferation than pure GG/SS 0% owing to the cell-adhesive capability of SS. We quantified the amount of dsDNA on day 3 and day 28 to characterize the effects of SS on cell proliferation (Figure 5B). The experiment results followed the same tendency as MTT assay data. As expected, ARPE-19 cells were able to proliferate in hydrogels including SS,[70] showing a higher quantity of dsDNA compared to that in GG/SS 0% hydrogels $p < 0.001$(***). Due to weight loss of hydrogels, all hydrogels showed a decrease of about 50% in the dsDNA content on day 28 compared to that on day 3. However, the GG/SS 0.5% hydrogel still showed the highest cell proliferation among hydrogels. In general, cell loss due to the weight loss in the hydrogels is unavoidable, and the gel should be gradually removed from the site of action after its purpose has been achieved.[9,71] As seen from the live/dead staining, ARPE-19 cells gradually spread and grew over time in all scaffolds, as indicated by green fluorescence (Figure 5C). However, dead cells were relatively increased in GG/SS 0% hydrogels compared to those in other hydrogels on 28 days of culture. The mechanism of how SS enhances cell proliferation has not yet been explained. However, as shown in previous studies, SS may enable cell−cell aggregation, suggesting that these cell−cell interactions could induce cell proliferation.[72] Therefore, it is expected that the addition of SS improves the limited cell attachment ability of GG,[73] promoting the proliferation and growth of ARPE-19 cells.

3.4.2. Gene Expression Analysis. To determine the gene expression level of ARPE-19 cells encapsulated in hydrogels, RT-PCR was performed with RPE-specific markers such as CRALBP, RPE65, RHODO, MITF, NPR-A, and COL I (Figure 6). CRALBP is a retinoid-binding protein abundantly expressed in RPE and Müller glia and thought to be involved in the retinal visual cycle.[74] RPE65 is the isomerase enzyme in RPE which is involved in the visual (retinoid) cycle, allowing optical pigments in photoreceptors, maintaining sight, and absorbing photons.[75] RHODO is the light receptor in rod photoreceptor cells of the retina associated with visual phototransduction.[76] MITF is essential for melanin production in melanocytes and regulates apoptosis through cell-cycle progression genes.[77,78] NPR-A controls gene expression related to RPE cell proliferation and sub-retinal fluid uptake.[79] COL I is a major component of retinal tissue involved in extracellular matrix formation.[80] Compared to GG/SS 0%, GG/SS 0.1% and GG/SS 0.5% displayed remarkably higher RPE-65 gene expression $p < 0.01$(**). Except for the RPE-65 gene, there was no significant difference in gene expression between the hydrogels; however, significant differences were found when p-values of GG/SS 0.05% and GG/SS 0.5% were calculated. In the four genes (CRALBP, RHODO, MITF, and NPR-A), GG/SS 0.05% had a p-value more than twice that of GG/SS 0.5%, and there was a 10-fold difference in COL expression. Therefore, the addition of SS is considered to play a positive role in ARPE-19 cell maturation, and in particular, GG/SS 0.5% hydrogels are thought to enhance the differentiation of RPE cells.[81]

4. CONCLUSIONS

Injectable GG/SS hydrogels were fabricated by blending various concentrations of SS to find the proper content of SS for retinal regeneration. An increase in the SS content resulted in a decrease in mass swelling and weight loss of the GG/SS hydrogels and an increase in the gelation temperature and injection force. However, it gave mechanical strength like that of retinal tissue and showed improvements in cytocompatibility and cell differentiation. In particular, the GG/SS 0.5% hydrogel had the most similar compressive strength to native retinal tissue (about 10 kPa) and exhibited more cell proliferation and differentiation ability for the ARPE-19 cells than other hydrogels. Consequently, the introduction of SS

https://doi.org/10.1021/acsomega.2c05113
ACS Omega 2022, 7, 41331−41340

enhanced the bioactivity of the GG/SS hydrogels and made GG/SS 0.5% hydrogels a promising biomaterial for retinal tissue engineering..

AUTHOR INFORMATION

Corresponding Author

Gilson Khang − *Department of Bionanotechnology and Bio-Convergence Engineering and Department of PolymerNano Science & Technology and Polymer Materials Fusion Research Center, Jeonbuk National University, Jeonju-si, Jeonbuk 54896, Republic of Korea; Department of Orthopaedic & Traumatology, Airlangga University, Kota SBY, Jawa Timur 60115, Indonesia;* orcid.org/0000-0002-6452-5653; Email: gskhang@jbnu.ac.kr

Authors

Soo in Kim − *Department of Bionanotechnology and Bio-Convergence Engineering, Jeonbuk National University, Jeonju-si, Jeonbuk 54896, Republic of Korea*

Ga Yeong Jeon − *Department of Bionanotechnology and Bio-Convergence Engineering, Jeonbuk National University, Jeonju-si, Jeonbuk 54896, Republic of Korea*

Se Eun Kim − *Department of Bionanotechnology and Bio-Convergence Engineering, Jeonbuk National University, Jeonju-si, Jeonbuk 54896, Republic of Korea*

Seung Ho Choe − *Department of Bionanotechnology and Bio-Convergence Engineering, Jeonbuk National University, Jeonju-si, Jeonbuk 54896, Republic of Korea*

Seung Jae Kim − *Department of Bionanotechnology and Bio-Convergence Engineering, Jeonbuk National University, Jeonju-si, Jeonbuk 54896, Republic of Korea*

Jin Sol Seo − *Department of Bionanotechnology and Bio-Convergence Engineering, Jeonbuk National University, Jeonju-si, Jeonbuk 54896, Republic of Korea*

Tae Woong Kang − *Department of Bionanotechnology and Bio-Convergence Engineering, Jeonbuk National University, Jeonju-si, Jeonbuk 54896, Republic of Korea*

Jeong Eun Song − *Department of Bionanotechnology and Bio-Convergence Engineering, Jeonbuk National University, Jeonju-si, Jeonbuk 54896, Republic of Korea;* orcid.org/0000-0001-6879-7616

Complete contact information is available at: https://pubs.acs.org/10.1021/acsomega.2c05113

Author Contributions

S.I.K. and G.Y.J. contributed equally to this work. All authors contributed to this manuscript and have given approval to the final version of the manuscript.

Notes

The authors declare no competing financial interest.

ACKNOWLEDGMENTS

This research was supported by Basic Science Research Program through the National Research Foundation of Korea (NRF) funded by the Ministry of Science, ICT and Future Planning (2020R1A2C2103089).

REFERENCES

(1) Lee, G. Y.; Kang, S. J.; Lee, S. J.; Song, J. E.; Joo, C. K.; Lee, D.; Khang, G. Effects of small intestinal submucosa content on the adhesion and proliferation of retinal pigment epithelial cells on SIS−PLGA films. *J. Regen. Med. Tissue Eng.* **2017**, *11*, 99−108.

(2) Chen, Y. M.; Liu, Z. Q.; Feng, Z. H.; Xu, F.; Liu, J. K. Adhesive protein-free synthetic hydrogels for retinal pigment epithelium cell culture with low ROS level. *J. Biomed. Mater. Res., Part A* **2014**, *102*, 2258−2267.

(3) Abedin Zadeh, M. A.; Khoder, M.; Al-Kinani, A. A.; Younes, H. M.; Alany, R. G. Retinal cell regeneration using tissue engineered polymeric scaffolds. *Drug Discovery Today* **2019**, *24*, 1669−1678.

(4) Gandhi, J. K.; Manzar, Z.; Bachman, L. A.; Andrews-Pfannkoch, C.; Knudsen, T.; Hill, M.; Schmidt, H.; Iezzi, R.; Pulido, J. S.; Marmorstein, A. D. Fibrin hydrogels as a xenofree and rapidly degradable support for transplantation of retinal pigment epithelium monolayers. *Acta Biomater.* **2018**, *67*, 134−146.

(5) Carido, M.; Zhu, Y.; Postel, K.; Benkner, B.; Cimalla, P.; Karl, M. O.; Kurth, T.; Paquet-Durand, F.; Koch, E.; Münch, T. A.; Tanaka, E. M.; Ader, M. Characterization of a mouse model with complete RPE loss and its use for RPE cell transplantation. *Invest. Ophthalmol. Visual Sci.* **2014**, *55*, 5431−5444.

(6) Lee, W.; Choi, J. H.; Lee, J.; Youn, J.; Kim, W.; Jeon, G.; Lee, S. W.; Song, J. E.; Khang, G. Dopamine-Functionalized Gellan Gum Hydrogel as a Candidate Biomaterial for a Retinal Pigment Epithelium Cell Delivery System. *ACS Appl. Bio Mater.* **2021**, *4*, 1771−1782.

(7) Hynes, S. R.; Lavik, E. B. A tissue-engineered approach towards retinal repair: scaffolds for cell transplantation to the subretinal space. *Albrecht Von Graefe's Arch. Clin. Exp. Ophthalmol.* **2010**, *248*, 763−778.

(8) Hunt, N. C.; Hallam, D.; Chichagova, V.; Steel, D. H.; Lako, M. The application of biomaterials to tissue engineering neural retina and retinal pigment epithelium. *Adv. Healthcare Mater.* **2018**, *7*, 1800226.

(9) Ballios, B. G.; Cooke, M. J.; van der Kooy, D.; Shoichet, M. S. A hydrogel-based stem cell delivery system to treat retinal degenerative diseases. *Biomaterials* **2010**, *31*, 2555−2564.

(10) Zhao, W.; Jin, X.; Cong, Y.; Liu, Y.; Fu, J. Degradable natural polymer hydrogels for articular cartilage tissue engineering. *J. Chem. Technol. Biotechnol.* **2013**, *88*, 327−339.

(11) Li, Y.; Yang, H. Y.; Lee, D. S. Advances in biodegradable and injectable hydrogels for biomedical applications. *J. Controlled Release* **2021**, *330*, 151−160.

(12) Catoira, M. C.; Fusaro, L.; Di Francesco, D.; Ramella, M.; Boccafoschi, F. Overview of natural hydrogels for regenerative medicine applications. *J. Mater. Sci.: Mater. Med.* **2019**, *30*, 115.

(13) Madl, A. C.; Myung, D. Supramolecular Host-Guest Hydrogels for Corneal Regeneration. *Gels* **2021**, *7*, 163.

(14) Liu, M.; Zeng, X.; Ma, C.; Yi, H.; Ali, Z.; Mou, X.; Li, S.; Deng, Y.; He, N. Injectable hydrogels for cartilage and bone tissue engineering. *Bone Res.* **2017**, *5*, 17014.

(15) Zia, K. M.; Tabasum, S.; Khan, M. F.; Akram, N.; Akhter, N.; Noreen, A.; Zuber, M. Recent trends on gellan gum blends with natural and synthetic polymers: A review. *Int. J. Biol. Macromol.* **2018**, *109*, 1068−1087.

(16) Zargar, S. M.; Mehdikhani, M.; Rafienia, M. Reduced graphene oxide−reinforced gellan gum thermoresponsive hydrogels as a myocardial tissue engineering scaffold. *J. Bioact. Compat Polym.* **2019**, *34*, 331−345.

(17) Sun, J.; Zhou, Z. A novel ocular delivery of brinzolamide based on gellan gum: in vitro and in vivo evaluation. *Drug Des. Dev. Ther.* **2018**, *Volume 12*, 383.

(18) Modi, D.; Nirmal, J.; Warsi, M. H.; Bhatia, M.; Hasan, N.; Kesharwani, P.; Jain, G. K. Formulation and development of tacrolimus-gellan gum nanoformulation for treatment of dry eye disease. *Colloids Surf., B* **2022**, *211*, 112255.

(19) Ranch, K.; Patel, H.; Chavda, L.; Koli, A.; Maulvi, F.; Parikh, R. K. Development of in situ ophthalmic gel of dexamethasone sodium phosphate and chloramphenicol: a viable alternative to conventional eye drops. *J. Appl. Pharm. Sci.* **2017**, *7*, 101−108.

(20) Xu, Z.; Li, Z.; Jiang, S.; Bratlie, K. M. Chemically modified gellan gum hydrogels with tunable properties for use as tissue engineering scaffolds. *ACS Omega* **2018**, *3*, 6998−7007.

(21) Gong, Y.; Wang, C.; Lai, R. C.; Su, K.; Zhang, F.; Wang, D.-a. An improved injectable polysaccharide hydrogel: modified gellan gum for long-term cartilage regeneration in vitro. *J. Mater. Chem.* **2009**, *19*, 1968−1977.
(22) Stevens, L.; Gilmore, K. J.; Wallace, G. G.; in het Panhuis, M. Tissue engineering with gellan gum. *Biomater. Sci.* **2016**, *4*, 1276−1290.
(23) Palumbo, F. S.; Federico, S.; Pitarresi, G.; Fiorica, C.; Giammona, G. Gellan gum-based delivery systems of therapeutic agents and cells. *Carbohydr. Polym.* **2020**, *229*, 115430.
(24) Song, Y.; Zhang, C.; Zhang, J.; Sun, N.; Huang, K.; Li, H.; Wang, Z.; Huang, K.; Wang, L. An injectable silk sericin hydrogel promotes cardiac functional recovery after ischemic myocardial infarction. *Acta Biomater.* **2016**, *41*, 210−223.
(25) Kunz, R. I.; Brancalhão, R. M. C.; Ribeiro, L. d. F. C.; Natali, M. R. M. Silkworm sericin: Properties and biomedical applications. *BioMed Res. Int.* **2016**, *2016*, 8175701.
(26) Mandal, B. B.; Priya, A. S.; Kundu, S. Novel silk sericin/gelatin 3-D scaffolds and 2-D films: fabrication and characterization for potential tissue engineering applications. *Acta Biomater.* **2009**, *5*, 3007−3020.
(27) Lamboni, L.; Gauthier, M.; Yang, G.; Wang, Q. Silk sericin: A versatile material for tissue engineering and drug delivery. *Biotechnol. Adv.* **2015**, *33*, 1855−1867.
(28) Nagai, N.; Murao, T.; Ito, Y.; Okamoto, N.; Sasaki, M. Enhancing effects of sericin on corneal wound healing in Otsuka Long-Evans Tokushima fatty rats as a model of human type 2 diabetes. *Biol. Pharm. Bull.* **2009**, *32*, 1594−1599.
(29) Nagai, N.; Fukuoka, Y.; Ishii, M.; Otake, H.; Yamamoto, T.; Taga, A.; Okamoto, N.; Shimomura, Y. Instillation of sericin enhances corneal wound healing through the ERK pathway in rat debrided corneal epithelium. *Int. J. Mol. Sci.* **2018**, *19*, 1123.
(30) Aramwit, P.; Yamdech, R.; Ampawong, S. Controlled release of chitosan and sericin from the microspheres-embedded wound dressing for the prolonged anti-microbial and wound healing efficacy. *AAPS J.* **2016**, *18*, 647−658.
(31) Kumar, J. P.; Bhardwaj, N.; Mandal, B. B. Cross-linked silk sericin−gelatin 2D and 3D matrices for prospective tissue engineering applications. *RSC Adv.* **2016**, *6*, 105125−105136.
(32) Eidet, J.; Reppe, S.; Pasovic, L.; Olstad, O.; Lyberg, T.; Khan, A.; Fostad, I.; Chen, D.; Utheim, T. The silk-protein sericin induces rapid melanization of cultured primary human retinal pigment epithelial cells by activating the NF-κB pathway. *Sci. Rep.* **2016**, *6*, 22671.
(33) Chirila, T. V.; Suzuki, S.; Bray, L. J.; Barnett, N. L.; Harkin, D. G. Evaluation of silk sericin as a biomaterial: in vitro growth of human corneal limbal epithelial cells on Bombyx mori sericin membranes. *Prog. Biomater.* **2013**, *2*, 14.
(34) Wang, Y.; Cai, R.; Tao, G.; Wang, P.; Zuo, H.; Zhao, P.; Umar, A.; He, H. A novel AgNPs/sericin/agar film with enhanced mechanical property and antibacterial capability. *Molecules* **2018**, *23*, 1821.
(35) Jo, Y. N.; Um, I. C. Effects of solvent on the solution properties, structural characteristics and properties of silk sericin. *Int. J. Biol. Macromol.* **2015**, *78*, 287−295.
(36) Zhang, Y.; Jiang, R.; Fang, A.; Zhao, Y.; Wu, T.; Cao, X.; Liang, P.; Xia, D.; Zhang, G. A highly transparent, elastic, injectable sericin hydrogel induced by ultrasound. *Polym. Test.* **2019**, *77*, 105890.
(37) Siritienthong, T.; Ratanavaraporn, J.; Aramwit, P. Development of ethyl alcohol-precipitated silk sericin/polyvinyl alcohol scaffolds for accelerated healing of full-thickness wounds. *Int. J. Pharm.* **2012**, *439*, 175−186.
(38) Karahaliloglu, Z.; Kilicay, E.; Denkbas, E. B. Antibacterial chitosan/silk sericin 3D porous scaffolds as a wound dressing material. *Artif. Cells, Nanomed., Biotechnol.* **2017**, *45*, 1172−1185.
(39) Saha, J.; Mondal, M.; Karim Sheikh, M.; Habib, M. Extraction, structural and functional properties of silk sericin biopolymer from Bombyx mori silk cocoon waste. *J. Text. Sci. Eng.* **2019**, *9*, 1000390.
(40) Fan, J. B.; Wu, L. P.; Chen, L. S.; Mao, X. Y.; Ren, F. Z. Antioxidant activities of silk sericin from silkworm Bombyx mori. *J. Food Biochem.* **2009**, *33*, 74−88.
(41) Chen, M. H.; Wang, L. L.; Chung, J. J.; Kim, Y.-H.; Atluri, P.; Burdick, J. A. Methods to assess shear-thinning hydrogels for application as injectable biomaterials. *ACS Biomater. Sci. Eng.* **2017**, *3*, 3146−3160.
(42) Salgado, A.; Coutinho, O. P.; Reis, R. L. Novel starch-based scaffolds for bone tissue engineering: cytotoxicity, cell culture, and protein expression. *Tissue Eng.* **2004**, *10*, 465−474.
(43) Liao, J.-L.; Yu, J.; Huang, K.; Hu, J.; Diemer, T.; Ma, Z.; Dvash, T.; Yang, X.-J.; Travis, G. H.; Williams, D. S.; Bok, D.; Fan, G. Molecular signature of primary retinal pigment epithelium and stem-cell-derived RPE cells. *Hum. Mol. Genet.* **2010**, *19*, 4229−4238.
(44) Livak, K. J.; Schmittgen, T. D. Analysis of relative gene expression data using real-time quantitative PCR and the 2− ΔΔCT method. *methods* **2001**, *25*, 402−408.
(45) Lamboni, L.; Xu, C.; Clasohm, J.; Yang, J.; Saumer, M.; Schäfer, K.-H.; Yang, G. Silk sericin-enhanced microstructured bacterial cellulose as tissue engineering scaffold towards prospective gut repair. *Mater. Sci. Eng., C* **2019**, *102*, 502−510.
(46) Wang, P.; Luo, Z.-g.; Xiao, Z.-g. Preparation, physicochemical characterization and in vitro release behavior of resveratrol-loaded oxidized gellan gum/resistant starch hydrogel beads. *Carbohydr. Polym.* **2021**, *260*, 117794.
(47) Lee, H.; Ahn, D.; Jeon, E.; Hui Fam, D. W.; Lee, J.; Lee, W. J. Macroscopic Assembly of Sericin toward Self-Healable Silk. *Biomacromolecules* **2021**, *22*, 4337−4346.
(48) Chen, C.-S.; Zeng, F.; Xiao, X.; Wang, Z.; Li, X.-L.; Tan, R.-W.; Liu, W.-Q.; Zhang, Y.-S.; She, Z.-D.; Li, S.-J. Three-dimensionally printed silk-sericin-based hydrogel scaffold: a promising visualized dressing material for real-time monitoring of wounds. *ACS Appl. Mater. Interfaces* **2018**, *10*, 33879−33890.
(49) Loh, Q. L.; Choong, C., *Three-Dimensional Scaffolds for Tissue Engineering Applications: Role of Porosity and Pore Size*; Mary Ann Liebert, Inc., 2013.
(50) Arango, M. C.; Álvarez-López, C. Effect of freezing temperature on the properties of lyophilized silk sericin scaffold. *Mater. Res. Express* **2019**, *6*, 095414.
(51) Krishna, L.; Nilawar, S.; Ponnalagu, M.; Subramani, M.; Jayadev, C.; Shetty, R.; Chatterjee, K.; Das, D. Fiber diameter differentially regulates function of retinal pigment and corneal epithelial cells on nanofibrous tissue scaffolds. *ACS Appl. Bio Mater.* **2020**, *3*, 823−837.
(52) Bružauskaitė, I.; Bironaitė, D.; Bagdonas, E.; Bernotienė, E. Scaffolds and cells for tissue regeneration: different scaffold pore sizes—different cell effects. *Cytotechnology* **2016**, *68*, 355−369.
(53) Kaberova, Z.; Karpushkin, E.; Nevoralová, M.; Vetrík, M.; Šlouf, M.; Dušková-Smrčková, M. Microscopic structure of swollen hydrogels by scanning electron and light microscopies: Artifacts and reality. *Polymers* **2020**, *12*, 578.
(54) Sievers, J.; Sperlich, K.; Stahnke, T.; Kreiner, C.; Eickner, T.; Martin, H.; Guthoff, R. F.; Schünemann, M.; Bohn, S.; Stachs, O. Determination of hydrogel swelling factors by two established and a novel non-contact continuous method. *J. Appl. Polym. Sci.* **2021**, *138*, 50326.
(55) Yoon, H. J.; Shin, S. R.; Cha, J. M.; Lee, S.-H.; Kim, J.-H.; Do, J. T.; Song, H.; Bae, H. Cold water fish gelatin methacryloyl hydrogel for tissue engineering application. *PLoS One* **2016**, *11*, No. e0163902.
(56) Worthington, K. S.; Wiley, L. A.; Bartlett, A. M.; Stone, E. M.; Mullins, R. F.; Salem, A. K.; Guymon, C. A.; Tucker, B. A. Mechanical properties of murine and porcine ocular tissues in compression. *Exp. Eye Res.* **2014**, *121*, 194−199.
(57) Silva, S. M.; Pinto, F. V.; Antunes, F. E.; Miguel, M. G.; Sousa, J. J.; Pais, A. A. Aggregation and gelation in hydroxypropylmethyl cellulose aqueous solutions. *J. Colloid Interface Sci.* **2008**, *327*, 333−340.
(58) Klouda, L.; Mikos, A. G. Thermoresponsive hydrogels in biomedical applications. *Eur. J. Pharm. Biopharm.* **2008**, *68*, 34−45.

https://doi.org/10.1021/acsomega.2c05113
ACS Omega 2022, 7, 41331−41340

(59) Zhu, L. J.; Arai, M.; Hirabayashi, K. Gelation of silk sericin and physical properties of the gel. *J. Seric. Sci. Jpn.* **1995**, *64*, 415−419.
(60) Jang, M. J.; Um, I. C. Effect of sericin concentration and ethanol content on gelation behavior, rheological properties, and sponge characteristics of silk sericin. *Eur. Polym. J.* **2017**, *93*, 761−774.
(61) Oliveira, J. T.; Martins, L.; Picciochi, R.; Malafaya, P.; Sousa, R.; Neves, N.; Mano, J.; Reis, R. Gellan gum: a new biomaterial for cartilage tissue engineering applications. *J. Biomed. Mater. Res., Part A* **2010**, *93*, 852−863.
(62) Palomino-Durand, C.; Lopez, M.; Cazaux, F.; Martel, B.; Blanchemain, N.; Chai, F. Influence of the Soluble−Insoluble Ratios of Cyclodextrins Polymers on the Viscoelastic Properties of Injectable Chitosan−Based Hydrogels for Biomedical Application. *Polymers* **2019**, *11*, 214.
(63) Xia, J.; Liu, Z.; Chen, Y.; Wang, Z.; Cao, Y. Fabrication of thermo-sensitive lignocellulose hydrogels with switchable hydrophilicity and hydrophobicity through an SIPN strategy. *RSC Adv.* **2019**, *9*, 29600−29608.
(64) Wang, P.; Li, X.; Zhu, W.; Zhong, Z.; Moran, A.; Wang, W.; Zhang, K.; Chen, S. 3D bioprinting of hydrogels for retina cell culturing. *Bioprinting* **2018**, *12*, No. e00029.
(65) Kundu, S. C.; Dash, B. C.; Dash, R.; Kaplan, D. L. Natural protective glue protein, sericin bioengineered by silkworms: potential for biomedical and biotechnological applications. *Prog. Polym. Sci.* **2008**, *33*, 998−1012.
(66) Park, C. J.; Ryoo, J.; Ki, C. S.; Kim, J. W.; Kim, I. S.; Bae, D. G.; Um, I. C. Effect of molecular weight on the structure and mechanical properties of silk sericin gel, film, and sponge. *Int. J. Biol. Macromol.* **2018**, *119*, 821−832.
(67) Noosak, C.; Jantorn, P.; Meesane, J.; Voravuthikunchai, S.; Saeloh, D. Dual-functional bioactive silk sericin for osteoblast responses and osteomyelitis treatment. *PLoS One* **2022**, *17*, No. e0264795.
(68) Baptista-Silva, S.; Borges, S.; Costa-Pinto, A. R.; Costa, R.; Amorim, M.; Dias, J. R.; Ramos, O.; Alves, P.; Granja, P. L.; Soares, R.; Pintado, M.; Oliveira, A. L. In situ forming silk sericin-based hydrogel: A novel wound healing biomaterial. *ACS Biomater. Sci. Eng.* **2021**, *7*, 1573−1586.
(69) Aramwit, P.; Kanokpanont, S.; Nakpheng, T.; Srichana, T. The effect of sericin from various extraction methods on cell viability and collagen production. *Int. J. Mol. Sci.* **2010**, *11*, 2200−2211.
(70) Khan, A. Z.; Utheim, T. P.; Moe, M. C.; Aass, H. C. D.; Sapkota, D.; Vallenari, E. M.; Eidet, J. R. The Silk Protein Sericin Promotes Viability of ARPE-19 and Induced Pluripotent Stem Cell-Derived Retinal Pigment Epithelial Cells in vitro. *Curr. Eye Res.* **2021**, *46*, 504−514.
(71) Spicer, C. D. Hydrogel scaffolds for tissue engineering: The importance of polymer choice. *Polym. Chem.* **2020**, *11*, 184−219.
(72) Cao, T.-T.; Zhang, Y.-Q. The potential of silk sericin protein as a serum substitute or an additive in cell culture and cryopreservation. *Amino Acids* **2017**, *49*, 1029−1039.
(73) Pacelli, S.; Paolicelli, P.; Petralito, S.; Subham, S.; Gilmore, D.; Varani, G.; Yang, G.; Lin, D.; Casadei, M. A.; Paul, A. Investigating the role of polydopamine to modulate stem cell adhesion and proliferation on gellan gum-based hydrogels. *ACS Appl. Bio Mater.* **2020**, *3*, 945−951.
(74) Xue, Y.; Shen, S. Q.; Jui, J.; Rupp, A. C.; Byrne, L. C.; Hattar, S.; Flannery, J. G.; Corbo, J. C.; Kefalov, V. J. CRALBP supports the mammalian retinal visual cycle and cone vision. *J. Clin. Investig.* **2015**, *125*, 727−738.
(75) Hauswirth, W. W.; Aleman, T. S.; Kaushal, S.; Cideciyan, A. V.; Schwartz, S. B.; Wang, L.; Conlon, T. J.; Boye, S. L.; Flotte, T. R.; Byrne, B. J.; Jacobson, S. G. Treatment of leber congenital amaurosis due to RPE65 mutations by ocular subretinal injection of adeno-associated virus gene vector: short-term results of a phase I trial. *Hum. Gene Ther.* **2008**, *19*, 979−990.
(76) Park, P. S.-H. Constitutively active rhodopsin and retinal disease. *Adv. Pharmacol.* **2014**, *70*, 1−36.
(77) Levy, C.; Khaled, M.; Fisher, D. E. MITF: master regulator of melanocyte development and melanoma oncogene. *Trends Mol. Med.* **2006**, *12*, 406−414.
(78) Wen, B.; Li, S.; Li, H.; Chen, Y.; Ma, X.; Wang, J.; Lu, F.; Qu, J.; Hou, L. Microphthalmia-associated transcription factor regulates the visual cycle genes Rlbp1 and Rdh5 in the retinal pigment epithelium. *Sci. Rep.* **2016**, *6*, 21208.
(79) Fujiseki, Y.; Omori, K.; Omori, K.; Mikami, Y.; Suzukawa, J.; Okugawa, G.; Uyama, M.; Inagaki, C. Natriuretic peptide receptors, NPR-A and NPR-B, in cultured rabbit retinal pigment epithelium cells. *Jpn. J. Pharmacol.* **1999**, *79*, 359−368.
(80) Campochiaro, P. A.; Jerdon, J.; Glaser, B. M. The extracellular matrix of human retinal pigment epithelial cells in vivo and its synthesis in vitro. *Invest. Ophthalmol. Visual Sci.* **1986**, *27*, 1615−1621.
(81) Ahmado, A.; Carr, A.-J.; Vugler, A. A.; Semo, C.; Gias, J. M.; Lawrence, L. L.; Chen, F. K.; Chen, P.; Turowski, L.; da Cruz, P. J.; Coffey, P. J. Induction of differentiation by pyruvate and DMEM in the human retinal pigment epithelium cell line ARPE-19. *Invest. Ophthalmol. Visual Sci.* **2011**, *52*, 7148−7159.

https://doi.org/10.1021/acsomega.2c05113
ACS Omega 2022, 7, 41331−41340